10/10/2021 3:40PM

The Impact of Image Processing Algorithms on Quantitative Optical Coherence Tomography Angiography Metrics in Diabetic Retinopathy

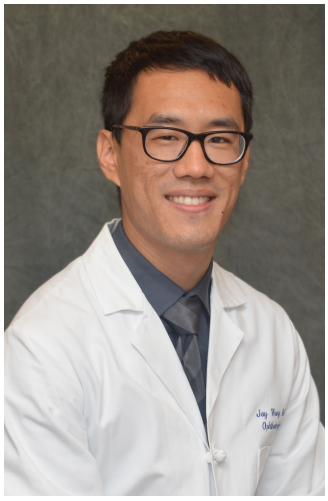

- Jay C Wang, MD
- Emily Li, MD
- Lucy Hui, MD
- Isaac Freedman, MPH
- Kristen Harris Nwanyanwu, MD, MBA, MHS

OBJECTIVE Does the use of different image processing algorithms to analyze optical coherence tomography angiography images impact not only quantitative metrics but also the conclusions of a particular study?

PURPOSE To evaluate the impact of using different image processing algorithms to calculate commonly reported quantitative metrics in optical coherence tomography angiography (OCTA) images in patients with various stages of diabetic retinopathy.

METHODS Single center, retrospective study of diabetic patients from September 2017 to December 2018. Ophthalmological exams and OCTA imaging with the Cirrus HD-OCT 5000 AngioPlex were performed. Patients with coexisting chorioretinal disease and scans of poor quality were excluded. Age, gender, visual acuity, stage of diabetic retinopathy (DR), and presence of diabetic macular edema (DME) were documented. 8 x 8 mm superficial slab images were thresholded using the Huang, Otsu, or Niblack algorithms in ImageJ. Vessel density (VD), skeletonized VD (SVD), and fractal dimension (FD) were calculated for each image. Mixed-effect uni- and multivariate linear regressions were performed.

RESULTS 301 scans from 104 patients were included. 90 were excluded for poor signal strength or significant artifact. Of the remaining 211, 67 had no DR, 99 had nonproliferative diabetic retinopathy (NPDR), and 45 had proliferative diabetic retinopathy

(PDR). 48 of 211 scans had DME. The thresholding algorithm used significantly impacted VD, SVD, and FD even when controlling for age, DME, and DR stage (all p-values < 0.001). The Otsu algorithm yielded significantly lower values for VD, SVD, and FD when compared to the Huang and Niblack algorithms (p-values < 0.001). On multivariate analysis, lower VD was significantly associated with DME but only with the Huang algorithm (p = 0.039) and PDR but only with the Niblack algorithm (p = 0.013). Lower SVD was significantly associated with PDR with all algorithms (p-values < 0.017) and DME but only with the Huang algorithm (p = 0.048). Lower FD was significantly associated with PDR with all algorithms (p-values < 0.026).

CONCLUSION Caution must be taken when quantitatively analyzing OCTA images, as the specific thresholding algorithm used may impact the conclusions of any given study. Fractal dimension may be a more robust metric less impacted by thresholding. There is a need for standardization of image processing algorithms to ensure robust and consistent analysis of OCTA imaging.

IRB APPROVAL No — I received a determination that the study/activity qualified for **exempt status or that it did not require IRB approval** from an IRB or another authorized oversight body *(IRB Exemption Letter may be requested)*.

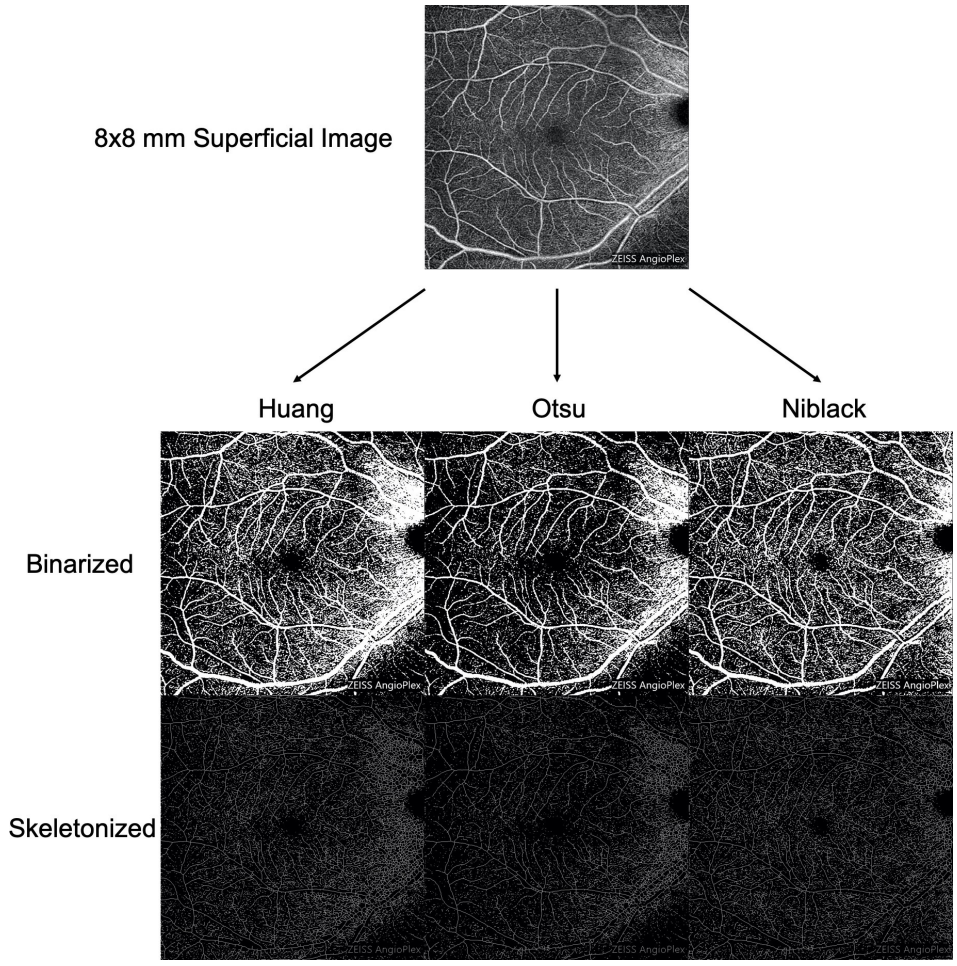

Top: Original 8x8 mm superficial image of a patient without diabetic retinopathy. Middle row: Binarized images using Huang, Otsu, and Niblack algorithms. Bottom row: Skeletonized images using Huang, Otsu, and Niblack algorithms.

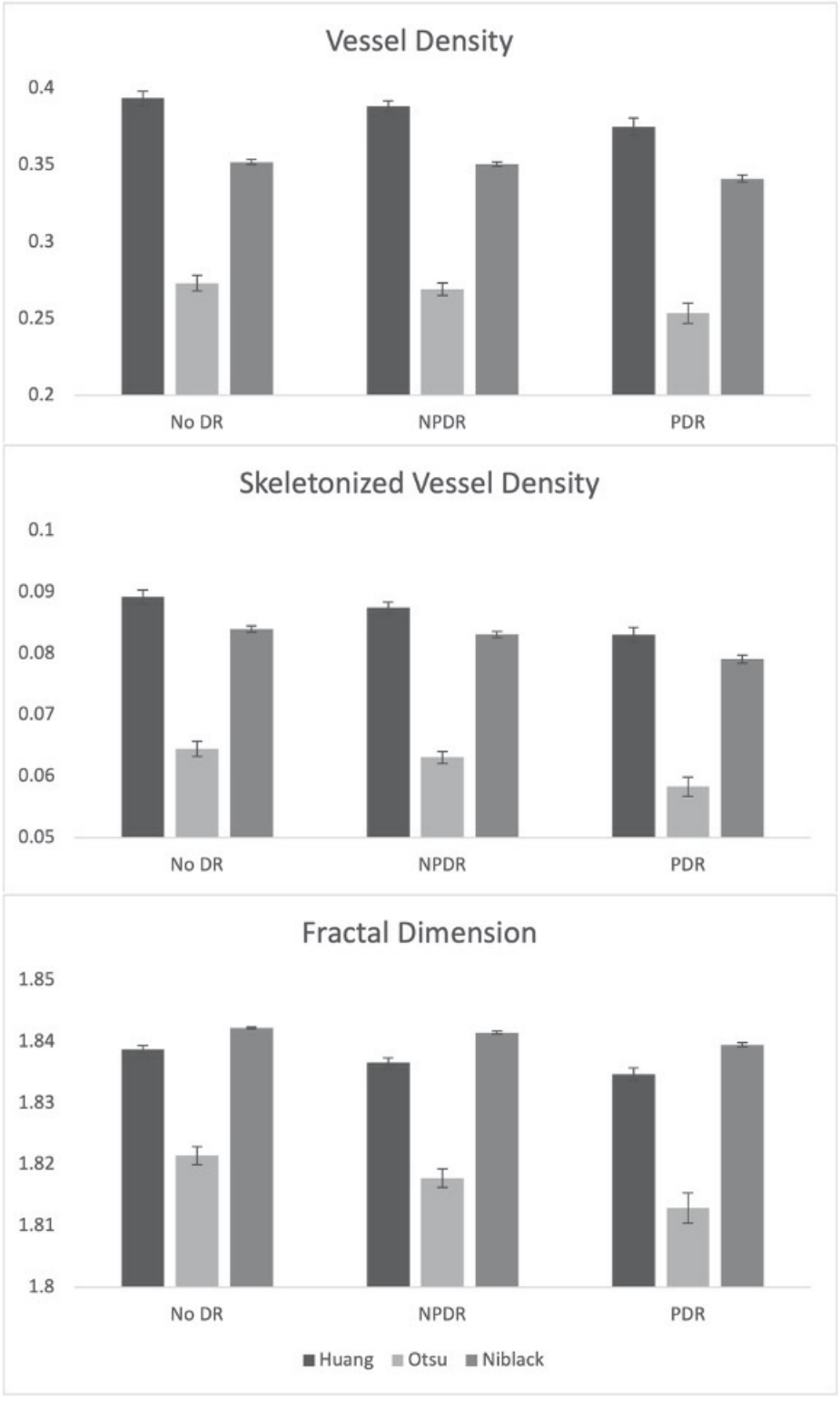

Bar graphs displaying the values of vessel density, skeletonized vessel density, and fractal dimension calculated using Huang, Otsu, and Niblack algorithms for patients with no DR (diabetic retinopathy), NPDR (nonproliferative diabetic reitnopathy), and PDR (proliferative diabetic retinopathy).

10/10/2021 3:46PM

Evaluation of Nonperfusion Area and Other Vascular Metrics by Widefield SS-OCTA as Biomarkers of Diabetic Retinopathy Severity

- John B. Miller, MD
- Itika Garg, MD
- Edward Lu
- Chibuike Kelechi Uwakwe
- Karen Wai, MD
- Raviv Katz, MS
- Ying Zhu, MD
- Jade Moon, BS
- Chloe Li
- Ines Lains, MD, MSc
- Dean Eliott, MD
- Tobias Elze, PhD
- Leo A. Kim, MD, PhD
- David M Wu, MD, PhD
- Joan W. Miller, MD
- Deeba Husain, MD
- Demetrios G. Vavvas, MD, PhD

OBJECTIVE WF SS-OCTA can be used for precise quantification of non-perfusion area (NPA) with high repeatability.

PURPOSE The current literature correlating widefield swept-source optical coherence tomography angiography (WF SS-OCTA) parameters with diabetic retinopathy (DR) severity is limited. We explore its value in a large cohort of diabetic patients in diagnosing and staging DR.

METHODS This was a prospective, cross-sectional observational study. We imaged all patients (November 2018-September 2020) using 6x6mm2 and 12x12mm2 scans centered on the fovea. Images were analyzed using the ARI Network and FIJI. Mixed effects multiple regression models and receiver operator characteristic analysis was used for

statistical analyses. The main outcome measures included vessel density (VD); vessel skeleton density (VSD); foveal avascular zone (FAZ) area, circularity and perimeter; and non-perfusion area (NPA).

RESULTS 473 eyes of 286 patients (69 eyes of 49 control patients and 404 eyes of 237 diabetic patients) were imaged. Among patients with diabetes (median age 59 years), 51 eyes had no DR, 185 eyes (88 mild, 97 moderate-severe) had non-proliferative DR (NPDR); and 168 eyes had proliferative DR (PDR). Trend analysis revealed a progressive decline in SCP VD and VSD, and increased NPA with increasing DR severity. Mild NPDR additionally had reduced VD and VSD in DCP. NPA was the best parameter to diagnose DR (AUC: 0.96), whereas all parameters combined on both scans efficiently diagnosed (AUC: 0.97) and differentiated between DR stages (AUC range: 0.83 - 0.97). The presence of diabetic macular edema was associated with reduced SCP and DCP VD and VSD within mild NPDR eyes, whereas an increased VD and VSD in SCP only among moderate-severe NPDR.

CONCLUSION Our work highlights the importance of NPA measured by WF SS-OCTA. Readily available, non-invasive, and repeatable, WF SS-OCTA is important tool for DR management. A combination of both 6x6mm2 and 12x12mm2 centered on fovea had the best diagnostic accuracy for DR and its staging. Further longitudinal studies are needed to assess NPA as a biomarker for progression or regression of DR severity.

IRB APPROVAL Yes — *IRB Approval Letter may be requested*.

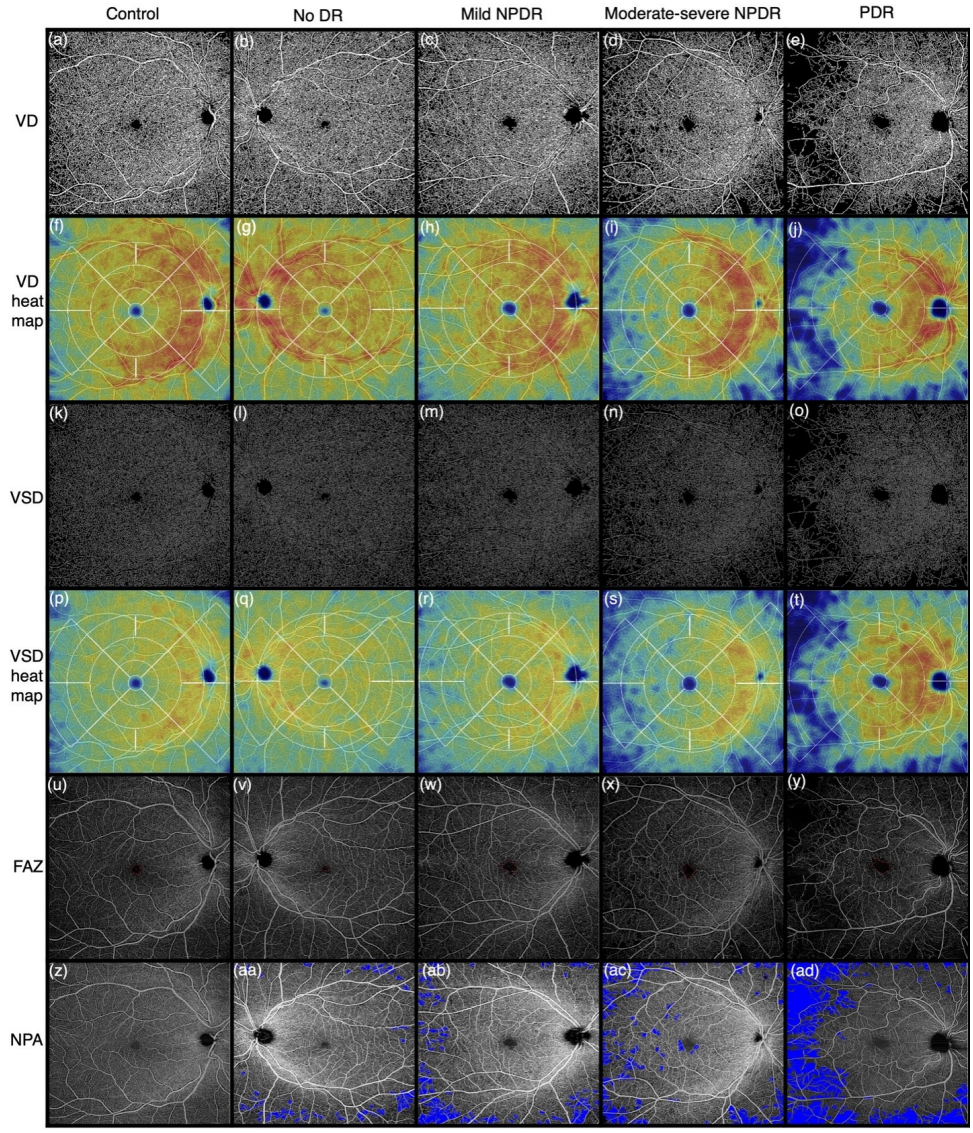

Representative full thickness 6x6 mm2 SS-OCTA scans VD (a-e): Binarized images from study groups. VD heat map (f-j): The color density maps with overlaying standardized ETDRS grid of the binarized images according to the VD distribution. VSD (k-o): Skeletonized images from different study groups. VSD heat map (p-t): The color density maps with overlaying standardized ETDRS grid of the skeletonized images according to the VSD distribution. FAZ (u-y): Representative images outlining the foveal avascular zone.

10/10/2021 3:52PM

Higher Order OCT Analysis for Inflammatory Signal Biomarkers in the HAWK Study

- Justis P. Ehlers, MD
- Kubra Sarici, MD
- Thuy K Le
- Leina Lunasco
- Jon Whitney
- Sudeshna Sil Kar, PhD
- Jamie Reese, RN
- Anant Madabhushi, PhD
- Sunil Srivastava, MD

OBJECTIVE To evaluate whether potential OCT biomarkers exist for characterizing or predicting intraocular inflammation using novel image analysis techniques following anti-VEGF treatment in the HAWK study.

PURPOSE To perform a comparative discovery assessment to evaluate the presence of OCT features that may precede or develop in association with intraocular inflammation (IOI), which might serve as potential OCT biomarkers for IOI and to evaluate image interrogation techniques for detection and characterization.

METHODS HAWK is a phase 3 study comparing brolucizumab to aflibercept in nAMD. A discovery-focused case-control OCT analysis was performed to evaluate potential OCT inflammatory biomarkers. This analysis included 34 eyes with an IOI event and 34 propensity-matched controls. This analysis includes comparative OCT feature assessment, radiomics evaluation, and machine learning characterization.

RESULTS OCT biomarker review by expert readers identified hyperreflective vitreous debris or preretinal hyperreflective deposits in 20 of 34 eyes with IOI (59%) compared to 1 of 34 eyes (3%) in the control group. In 9 of 20 eyes with qualitative OCT findings, these features were identified at visits prior to the IOI reported event. Machine learning quantitative characterization of the vitreous compartment identified differences in the

number of hyperreflective vitreous and preretinal foci between eyes in the IOI group and the control group, including prior to the IOI reported event. Radiomics assessment of the vitreous identified distinct texture signatures and alterations in eyes in the IOI group that were able to be used to distinguish between eyes in the IOI and control groups.

CONCLUSION In this preliminary discovery evaluation in the HAWK dataset, OCT biomarkers were identified that may facilitate identification of eyes at-risk for developing IOI related events. Further analysis is needed to confirm these findings. Next generation platforms for image characterization and feature extraction may enable early stratification of IOI risk.

IRB APPROVAL Yes — *IRB Approval Letter may be requested*.

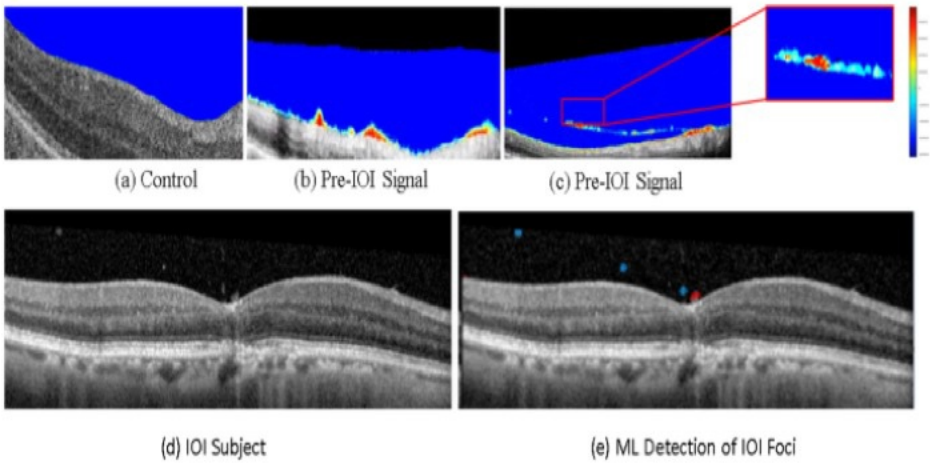

Radiomics and Machine Learning Feature Extraction of Inflammatory OCT Biomarkers. Radiomics assessment of vitreous compartment texture features in control (a) and IOI subjects (b-c). Enhanced textural features (light blue/yellow/red) are identified prior to actual IOI event (b,c). Automated machine learning IOI feature detection (d,e). B-scan in IOI subject demonstrating vitreous debris and preretinal deposits prior to IOI event (d). ML feature detection with overlayof vitreous debris (blue) and preretinal deposits (red) enabling quantification IOI biomarkers.

10/10/2021 4:04PM

Evaluation of Real-Time Volumetric (4D) and B-Scan Images Acquired With Microscope Integrated OCT on a 3D Platform During Human Vitreoretinal Surgery

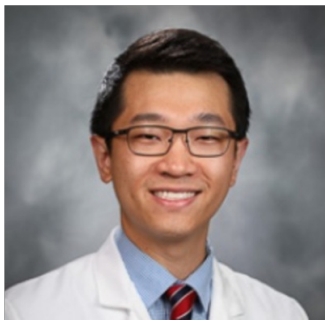

- Henry L Feng, MD
- Jianwei David Li
- William Raynor
- Christian Viehland
- Joseph A Izatt, PhD
- Cynthia Ann Toth, MD
- Lejla Vajzovic, MD, FASRS

OBJECTIVE To evaluate agreement between real-time volumetric (4D) and B-scan images acquired with microscope integrated OCT (MI-OCT) and 3D microscope video captured during surgery on the NGenuity platform.

PURPOSE Intraoperative identification and manipulation of preretinal tissue are essential for surgical removal. We aim to determine the relationship between real-time volumetric and B-scan images acquired with MI-OCT and 3D microscope video captured on the Ngenuity platform in adult human eyes that underwent vitreoretinal surgery for epiretinal membrane.

METHODS Prospective translational study of 9 adult human eyes that underwent vitreoretinal surgery for epiretinal membrane with visualization from an investigational swept-source MI-OCT system included in a unified heads-up display on the NGenuity 3D platform. Surgical video clips extracted from Ngenuity were graded by 2 retina specialists for presence of preretinal membranes and intraocular instruments, and evidence of membrane manipulation. Graders first evaluated MI-OCT volumetric and B-scan video sequences only, followed by corresponding 3D microscope videos only in a randomized order. Positive and negative percent agreement (PPA, NPA) were calculated for MI-OCT findings compared to 3D video.

RESULTS In 30 NGenuity video clips (mean duration 13.1 +/- 3 seconds), retinal surface was discernable in 100% of MI-OCT sequences. Aggregate PPA was 91.7% for presence of preretinal membranes, 96.6% for presence of intraocular instruments, and 84% for

evidence of membrane manipulation. NPA was 100% for no intraocular instruments and 80% for no membrane manipulation; there were 2 instances of membrane manipulation identified on MI-OCT but not on 3D video. Preretinal membranes were identified on one or both modalities in all sequences, therefore NPA could not be calculated for this finding. Interrater reliability was moderate on MI-OCT and near perfect on 3D video (Cohen's Kappa 0.366 and 1.000 for membranes, 0.474 and 1.000 for instrument, and 0.500 and 0.870 for membrane manipulation, respectively). Differences in interrater reliability may reflect varying degrees of familiarity with the MI-OCT system in terms of instrument visibility, shadowing, or lack of stereo projection of OCT volumes.

CONCLUSION MI-OCT volumetric and B-scan images accurately identified preretinal membranes, intraocular instruments, and instances of membrane manipulation corresponding to the 3D microscope view on the NGenuity platform in real-time during human vitreoretinal surgery. Further evaluation is warranted to explore the synergy of both MI-OCT and stereoscopic 3D video on a unified heads-up display.

IRB APPROVAL Yes — *IRB Approval Letter may be requested*.

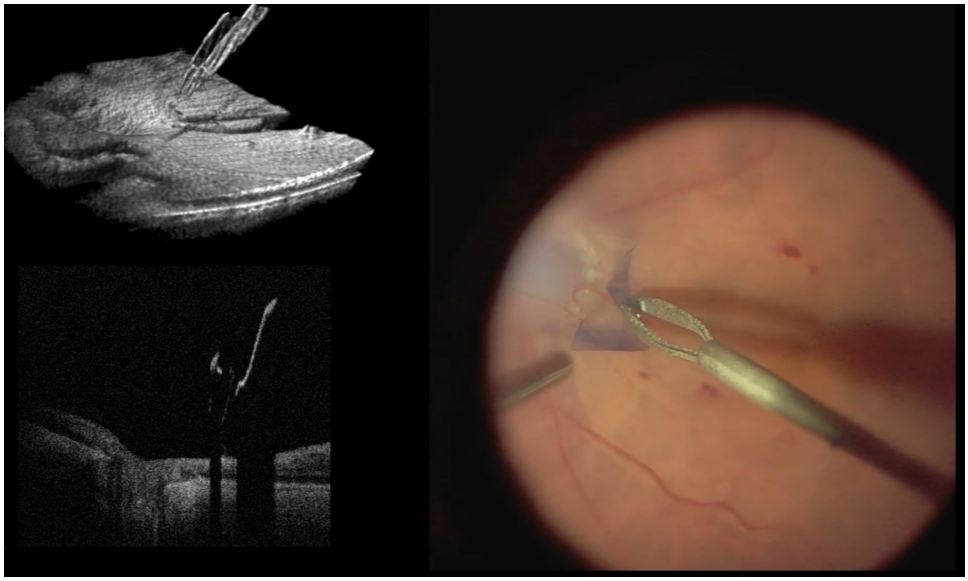

Representative image of the MI-OCT volume scan (A), B-scan (B), and stereoscopic 3D video (C) on a unified heads-up display.

10/10/2021 4:10PM

Commercial OCT Enters the Cellular Age – Tracking Macrophage Surveillance of the Macula Circulation!

- Richard B. Rosen, MD, DSc(Hon), FACS, FASRS, FARVO
- Oscar Otero-Marquez, MD
- Maria V Castanos Toral, MD
- Davis B Zhou, BS
- Rishard Weitz
- Alfredo Dubra, PhD
- Justin Migacz, PhD
- Toco Chui, PhD

OBJECTIVE To evaluate the ability of commercial OCT to image and measure single cell inflammatory response to retinal vascular disease.

PURPOSE Macrophages at the retinal surface act as sensors and regulators of vascular and neuronal tissue and could serve as biomarkers of disease onset and severity. Here we demonstrate the ability of a commercial OCT to image these immune cells in vascular disorders, previewing a new era of clinical cellular diagnostics.

METHODS 71 patients with various ischemic retinopathies (49 eyes with DR, 12 eyes with SCR and 10 eyes with RVO) and 14 controls were imaged using a clinical SD-OCT (Avanti RTVue-XR; Optovue). Ten 3x3mm scans centered at the fovea were acquired and averaged. FAZ borders were outlined manually on the OCT-A scan. Automated surface macrophage cell density measurements within the FAZ were performed on the 3µm OCT-reflectance (OCT-R) slab above the ILM surface using a novel MATLAB application. Surface macrophage cell density maps were also generated for each subject. OCT-A full vascular slab, including the ILM to 9µm below the posterior boundary of the OPL, was used to measure capillary density.

RESULTS Surface macrophage cells within the FAZ were found in 80% of diabetic eyes, 86% of SCR eyes and 90% of RVO eyes, but only 31% of controls. Statistically significant differences in surface macrophage cell densities were observed between ischemic

vasculopathy groups and controls (Kruskal-Wallis tests, P= 0.0005) with mean±SDs of 5±5, 6±7, 13±10 and 1±1 cells/mm2 in SCR, DR ,RVO, and control groups, respectively. A significant inverse correlation between surface macrophage cell densities within the FAZ and perifoveal perfused capillary densities was shown using linear regression (R= -0.22, P= 0.037).

CONCLUSION Clinical OCT is capable of imaging and measuring macular surface macrophage cells, and offers a new clinical biomarker for tracking initiation and progression of retinal vascular disease and response to therapy. Higher surface macrophage cell densities within the FAZ appear to correlate with progressive reduction of surrounding perfused capillary density as ischemic burden worsens.

IRB APPROVAL Yes — *IRB Approval Letter may be requested*.

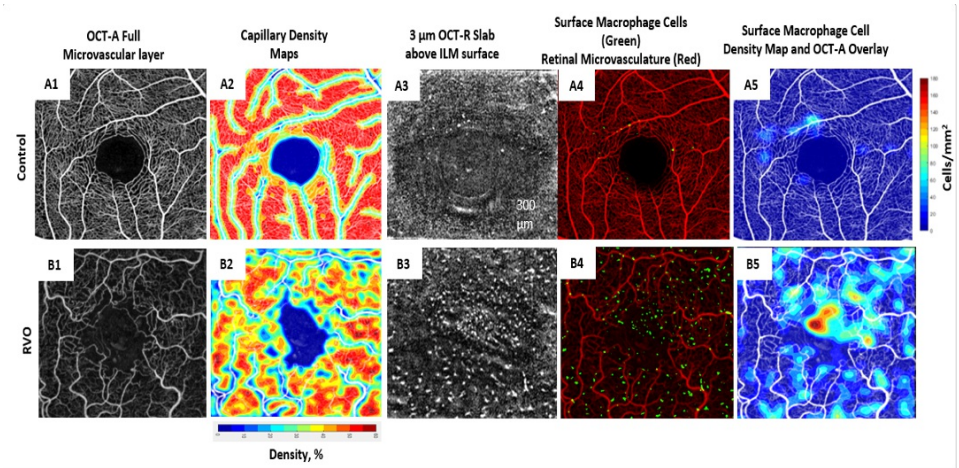

Macular Surface Macrophages Cells and Microvasculature in a Control (top row), and RVO patient (bottom row) using clinical OCT :A1& B1) OCT-A full vascular layer. A2 & B2) 3 µm OCT-R slab located above the ILM surface highlighting cells. A3 & B3) Overlay of A1, B1, (green) onto A2& B2 (red). A4 & B4) Overlay of Surface Macrophage Density Map and OCT-A.

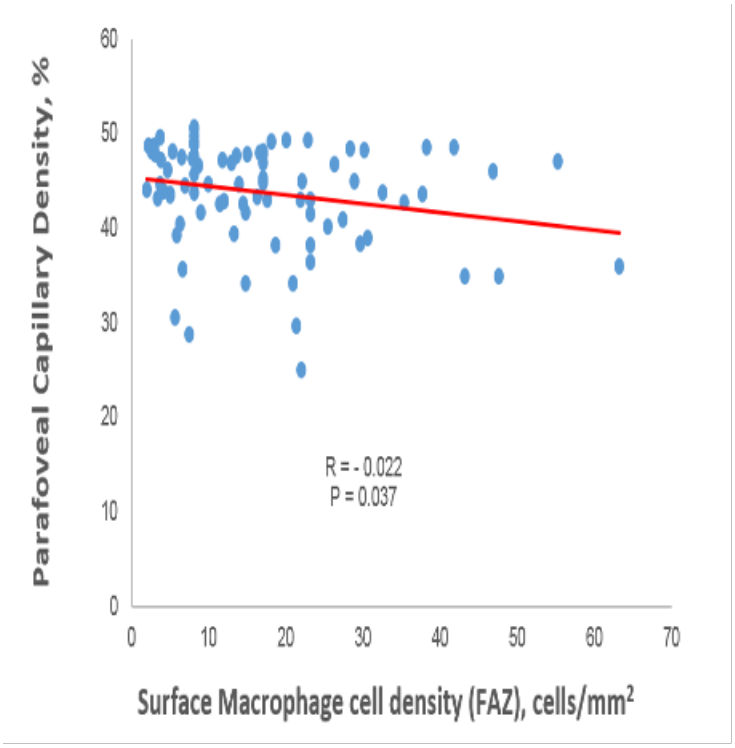

FAZ Macrophage Cell Density and Perifoveal Capillary Density show a significant inverse correlation (R=-0.22, p==0.037) using Pearson's method.

10/10/2021 4:16PM

Characterization and Diagnosis of Retinoschisis and Schisis Detachments Using Spectral Domain Optical Coherence Tomography

- Rohan A Jalalizadeh, MD
- Bradley T. Smith, MD

OBJECTIVE The aim of this study was to demonstrate clinical utility of spectral domain OCT (SD-OCT) in the diagnosis of acquired retinoschisis and to better characterize features of retinoschisis.

PURPOSE The diagnosis and management of peripheral and macular retinoschisis can be significantly aided by proper use of SD-OCT. This study characterizes findings in a large series of eyes with retinoschisis. In particular, the rate of schisis detachment in cases of peripheral retinoschisis is investigated, as well as frequency of macular involvement in cases of peripheral retinoschisis.

METHODS In this retrospective, cross-sectional, descriptive study, billing codes were used to identify consecutive patients with a diagnosis of retinoschisis seen by one physician in a private practice over the past 10 years. The proportion of eyes with peripheral retinoschisis, schisis detachment, and macular retinoschisis was determined. Quadrant of involvement, inner and outer wall breaks, and layers involved were recorded based on SD-OCT and clinical examination. Cases in which the patient was determined to have a diagnosis other than retinoschisis were excluded, and eyes for which SD-OCT was not of sufficient quality were excluded from the pertinent analysis.

RESULTS 270 eyes of 184 patients were included in the study. Of all eyes, 194 (71.9%) had peripheral retinoschisis and 15 (5.6%) had a schisis detachment. No eyes were found to have a retinal detachment alone. Macular retinoschisis was present in 57 (21.1%) eyes, and combined macular and peripheral retinoschisis in 5 (1.9%) eyes. Of the subset of eyes excluding macular retinoschisis, 93.0% had peripheral retinoschisis and 7.0% had schisis detachment. Of eyes with peripheral retinoschisis without schisis detachment, inner wall breaks were detected in 4 (2.1%) and outer wall breaks were detected in 23 (11.9%). In eyes with peripheral retinoschisis, splitting occurred in the outer plexiform layer in 60.0%, the retinal nerve fiber layer in 10.0%, a combination of layers in 22.5%, and indeterminate in 7.5%. Location of peripheral involvement was inferotemporal in 58.3%, superotemporal in 14.9%, temporal in 14.3%, and inferior in 12.0%.

CONCLUSION SD-OCT successfully verified clinical diagnosis of retinoschisis in all eyes, aided in therapeutic decision-making by identifying the presence of schisis detachment and location and layer of breaks, and contributed to understanding of pathogenesis and natural history of retinoschisis by demonstrating the layer of splitting. This series represents the largest such descriptive study to date.

IRB APPROVAL Yes — *IRB Approval Letter may be requested*.

	Number (n = 270)	Proportion of Total Eyes
Peripheral Retinoschisis	194	71.9 %
Schisis Detachment	15	5.6 %
Macular retinoschisis	57	21.1 %
Macular + Peripheral Retinoschisis	5	1.9 %

Table 1: Distribution of Retinoschisis Among Consecutive Cases

10/10/2021 4:26PM

Feasibility and Clinical Utility of Ultra-Widefield Navigated Swept-Source Optical Coherence Tomography Imaging

- Kyle D Kovacs, MD
- Luis A Gonzalez, MD, MPH
- Benjamin W Botsford, MD
- Tamara L Lenis, MD, PhD
- Anton Orlin, MD
- Thanos Papakostas, MD
- Donald J. D'Amico, MD
- Abdallah Mahrous, MD
- Mike Ryan, MD
- Szilárd Kiss, MD

OBJECTIVE To evaluate the clinical utility and feasibility of a novel scanning laser ophthalmoscope-based navigated ultra-widefield swept-source optical coherence tomography (UWF SS-OCT) imaging system.

PURPOSE To characterize implementation of UWF SS-OCT in routine clinical practice by: 1) describing the cohort of patients and anatomic findings that underwent UWF SS-OCT; 2) assessing the logistics of image acquisition and interpretability; 3) determining which imaging indications offered insightful clinical information about the abnormality at hand, helping guide clinical management.

METHODS Retrospective, single-center, consecutive case series of patients evaluated between September 2019 and October 2020 with UWF SS-OCT (modified Optos P200TxE, Optos PLC, Dunfermline, Scotland) as part of routine retinal care. Logistics of image acquisition were assessed including: duration of image capture; percentage of interpretable images obtained; and diagnostic interpretability of images based on blind review of images by two independent graders; the nature of the peripheral abnormality captured; and clinical utility in management decisions.

RESULTS Eighty-two eyes from 72 patients were included. Patients were 59.4 ± 17.1 years of age (range 8 to 87 years). During imaging, 4.4 series of images were obtained in 4.1 minutes, with 86.4% of the image series deemed to be diagnostic of the peripheral pathology on blinded image review. The most common pathologic findings were

chorioretinal scars (18 eyes). In 31 (38%) eyes, these images were meaningful in supporting clinical decision making with definitive findings. Diagnoses imaged included: retinal detachment combined with retinoschisis, retinal hole with overlying vitreous traction and subretinal fluid, vitreous inflammation overlying a peripheral scar, Coats' disease, and peripheral retinal traction in sickle cell retinopathy.

CONCLUSION Navigated UWF SS-OCT imaging was clinically practical, providing high quality characterization of peripheral retinal lesions for all eyes. Images directly contributed to management plans for a clinically meaningful set of patients (38%). Future studies should further assess the value of this imaging modality and its role in diagnosing, monitoring and treating peripheral lesions.

IRB APPROVAL Yes — *IRB Approval Letter may be requested*.

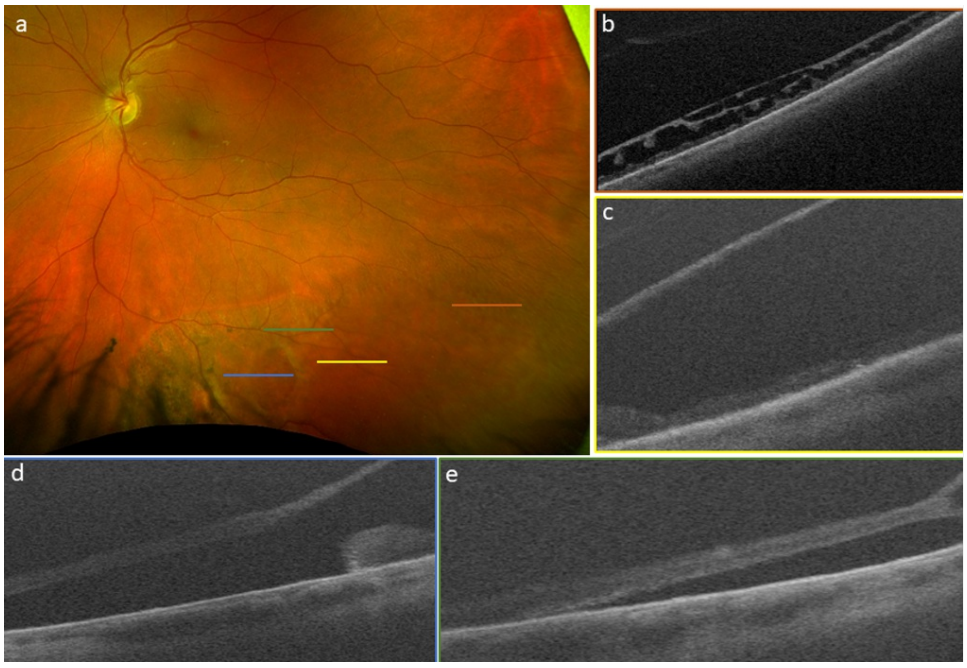

Pseudocolor image (a) demonstrating retinoschisis with large cavity, outer retinal break, associated retinal detachment, without inner retinal break. UWF SS-OCT revealed shallow retinoschisis temporally (b, orange), bullous retinoschisis cavity (c, yellow), outer retinal break with rolled margins (d, blue), with subretinal fluid nasal and posterior to retinoschisis cavity (e, green).

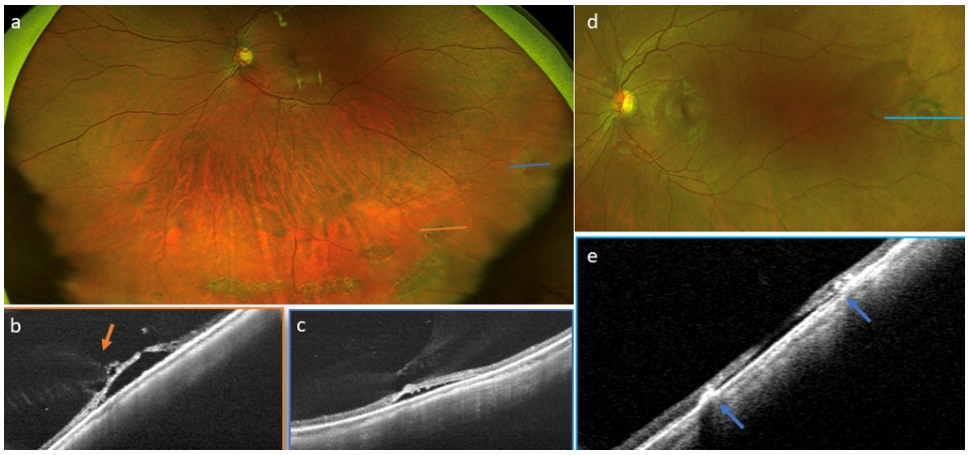

Pseudocolor image (a) of inferior lattice and atrophic holes (b, orange and c, blue) with subretinal fluid and vitreous traction (orange arrow). Laser retinopexy performed in this symptomatic patient, supported by vitreous traction on OCT. Pseudocolor image (d) of pigmented retinal hole, flat on OCT (e, blue) with no traction and scarred down edges (blue arrows). The patient was observed.

10/10/2021 4:30PM

One-Year Outcome and Predictors of Treatment Outcome in Central Serous Chorioretinopathy: Multimodal Imaging Based Analysis

- SUPRIYA ARORA, MS
- Dmitri S Maltsev, MD, PHhD
- Sumit Randhir Singh
- Niroj Kumar Sahoo, MD
- Deepika Parmeshwarappa, MD
- Mahima Jhingan, MD
- Tarun Arora, MD
- Alexei N Kulikov, DSc
- Claudio Iovino
- M. N Ibrahim, B Tech
- Filippo Tatti, MD
- Ramkailash Gujar, B Optom
- Ramesh Venkatesh, MS
- Nikitha Reddy, MS
- Dinah Zur, MD
- Gilad Fainberg, MD
- Ram Sneith, DNB
- Enrico Peiretti, MD
- Marco Lupidi, MD
- Jay Chhablani, MD

OBJECTIVE Evaluation of follow up and treatment outcome of central serous chorioretinopathy based on the new multimodal imaging-based classification and identify the predictors for anatomic and visual outcome.

PURPOSE To study the follow up and treatment outcome of central serous chorioretinopathy (CSCR) based on the new multimodal imaging-based classification and identify the predictors for anatomic and visual outcome.

METHODS Retrospective, multicentric study on 95 eyes of 93 patients diagnosed with CSCR and available examination and multimodal imaging at baseline, 3 months, 6 months

and 12 months were included. Eyes with macular neovascularization, atypical CSCR or any other disease were excluded. Eyes were classified by two masked retina specialists as per the new CSCR classification at baseline and every follow up into i) simple/ complex CSCR ii) primary episode/ recurrence/ resolved CSCR iii) persistent subretinal fluid (SRF)(> 6 months) or not iv) outer retinal atrophy present or absent and v) fovea involved or not. Statistical analysis was performed using MedCalc 18.4.1 (MedCalc Software, Ostend, Belgium).

RESULTS At the baseline, observation was advised to 70% eyes with simple CSCR whereas photodynamic therapy was performed in 49% eyes with complex CSCR. Over the follow up, decrease in central macular thickness (CMT) was higher in simple CSCR as compared to complex CSCR (p=0.008) and the recurrences were more in eyes with lower CMT at baseline (p=0.0002). Median time of resolution of SRF was 3 months and 6 months in simple and complex CSCR eyes respectively (p=0.09). For the 12 months follow up, median fluid free period was greater(p=0.03) while number of interventions performed was lesser in eyes with simple CSCR as compared to complex CSCR (p=0.006). On univariate analysis, there was a significant association between best corrected visual acuity (BCVA) and CMT at baseline with BCVA at 12 months (p<0.0001,p=0.002). Multiple regression analysis showed baseline BCVA and baseline persistent SRF to be predictive of BCVA at 12 months (p<0.0001) and persistent SRF at 12 months (p=0.04) respectively.

CONCLUSION Complex CSCR more often required photodynamic therapy, was associated with shorter fluid free interval and longer time for SRF resolution. Baseline BCVA and persistent SRF were predictive of final visual and anatomical outcome. The new multimodal imaging based classification is helpful in establishing objective criteria for planning treatment approaches for CSCR.

IRB APPROVAL Yes — *IRB Approval Letter may be requested*.

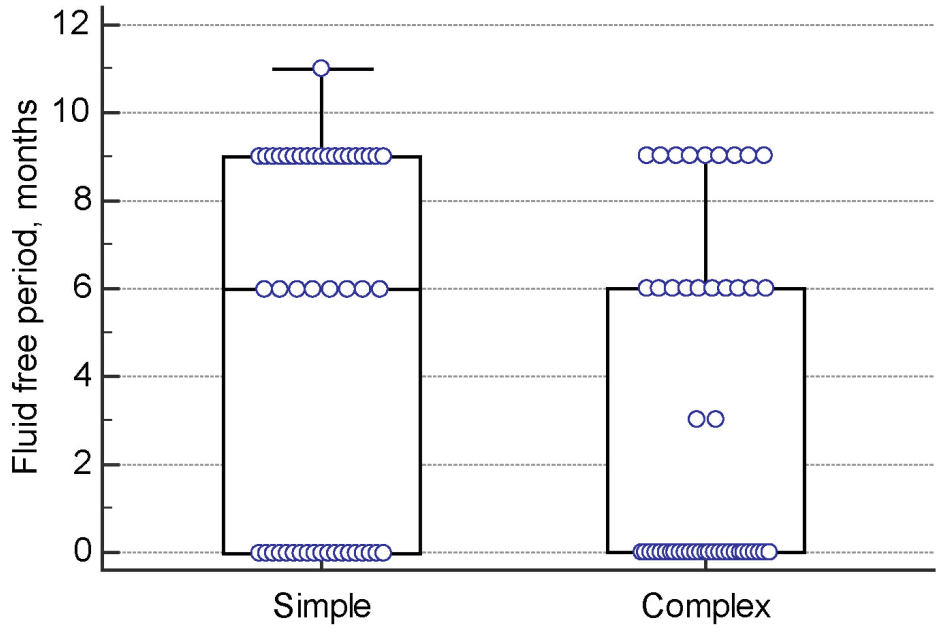

Fluid free period in simple versus complex central serous chorioretinopathy (CSCR). Median fluid free period was significantly greater in eyes with simple CSCR [6 (0.0-9.0) months] as compared to complex CSCR [0 (0.0-6.0) months] (p=0.03) over 12 months follow up. Inner horizontal line shows the median value. Each case is presented as a circle.

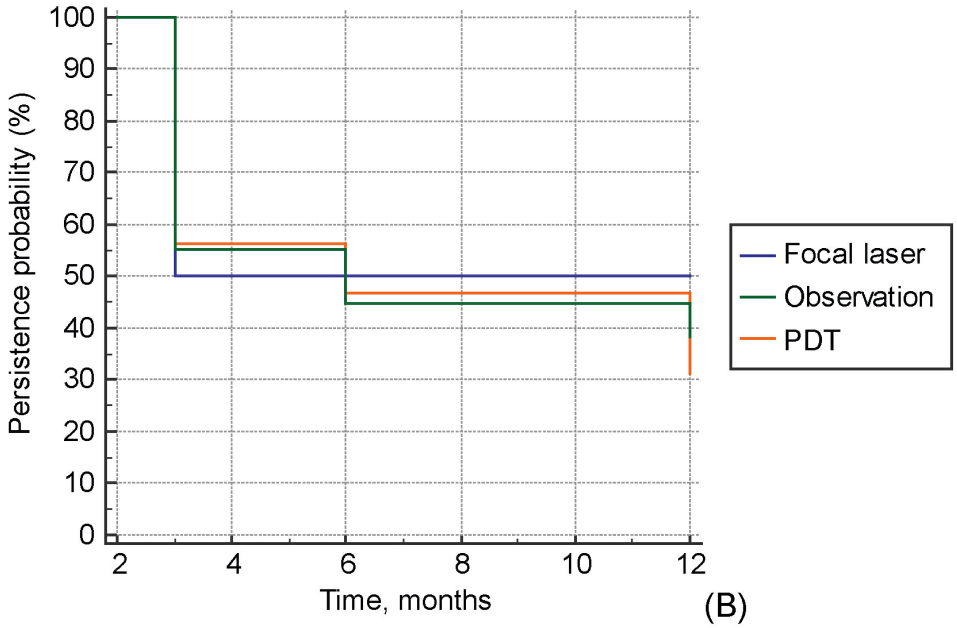

Kaplan-Meier curve demonstrating probability of persistence of subretinal fluid with different treatment options over a period of 12 months. The persistence probability after 12 months as determined from Kaplan-Meier analysis was 31.3%, 38.3% and 50% in the photodynamic therapy (PDT), observation and focal laser treatment respectively. Comparison of survival curves (persistence probability) with log-rank test showed no statistically significant difference (p=0.68) between different treatment options.

10/10/2021 4:34PM

OCT-A Findings in Pediatric Retina

- Audina M. Berrocal, MD FASRS
- Prashanth G Iyer, MD, MPH
- Nimesh A. Patel, MD
- Julia Hudson, MD
- Nicolas A Yannuzzi, MD

OBJECTIVE To look at the experience of intraoperative OCTA in a busy pediatric retina practice in a tertiary center.

PURPOSE To describe new findings of pediatric retinal disorders with the use of OCTA.

METHODS IRB approved retrospective review of 120 pediatric patients who underwent OCTA of both eyes (when possible). Study started in 2018 to the present. All patients went to the operating room for evaluation under anesthesia for diagnosis, treatment, follow up or surgical repair.

RESULTS We analyzed AF, OCT and OCTA of all patients. We looked at Coats disease, FEVR, Incontinential pigmenti, trauma, retinal detachments (myopia/Stickler syndrome), Marfan, Best disease, chorioretinal coloboma, X-linked retinoschisis, optic pit, PFV and ROP.

CONCLUSION AF, OCT and OCTA are important test in the diagnosis and management of pediatric retinal diseases. We have seen certain traits in each disease not described before. It is obviously important to do these tests under anesthesia due to the poor cooperation of children while awake.

IRB APPROVAL Yes — *IRB Approval Letter may be requested*.

10/10/2021 4:38PM

Recognizable Patterns of Submacular Fibrosis in the Enhanced S-Cone Syndrome

- Sawsan R Nowilaty, MD, FASRS
- Abrar Khalid Alsalamah
- Abdullah Abu Bakar, MD
- Patrik Schatz, MD, PhD
- Arif O. Khan, MD

OBJECTIVE To describe the recurrent patterns of subretinal fibrosis observed in enhanced S-cone syndrome (ESCS) and emphasize that these patterns by themselves are strongly suggestive for the diagnosis of ESCS.

PURPOSE To highlight, describe the distinguishing features and classify the recurrent recognizable patterns of subretinal fibrosis in ESCS, based on 47 consecutive patients with submacular fibrosis identified from 101 consecutive ESCS patients seen over a 27-year period, and emphasize that these patterns by themselves strongly suggest an underlying diagnosis of ESCS.

METHODS Retrospective case series of 101 consecutive patients with ESCS of which 47 patients with subretinal fibrosis were identified. Diagnosis of ESCS was based on clinical features supported by pathognomonic electroretinography (ERG) findings and/or genetic analysis in over 92% of cases. Collected data included macular spectral domain optical coherence tomography (OCT) scans, color fundus imaging, fluorescein angiography, full-field standard ERG and results of molecular genetic testing. The patterns of subretinal fibrotic lesions were examined, described with their angiographic and OCT features, and correlated with the genetic findings.

RESULTS Of 101 patients with ESCS, 47 (46.5%; 24 males; 36 unrelated consanguineous families; 85 eyes) had subretinal fibrosis. Mean age at presentation was 14 years. Best-corrected visual acuity ranged from 20/20 to hand motion. All 34 genetically-tested patients were homozygous for pathogenic NR2E3 variants. Subretinal fibrosis was always in the macular area, although it extended beyond in some cases. Six recurrent patterns of submacular fibrosis were noted: central unifocal nodular (22%), circumferential unifocal nodular (7%), multifocal nodular (37%), arcuate (21%), helicoid (4%), and thick geographic (11%). 27% of eyes had a combination of patterns. Fibrotic lesions were sharply-defined, bright with deep gray pigmentation and surrounded by a characteristic halo. Previous misdiagnosis as inflammatory disease was common. Fibrosis was fairly symmetrical in a given patient but not always present or identical in other affected individuals with a given mutation from the same or different family

CONCLUSION These recognizable patterns of submacular fibrosis are part of the ESCS phenotypic spectrum and strongly suggest the disease. Recognizing these patterns as phenotypic features of ESCS is important, because misdiagnosis as inflammatory disease is

common and awareness can spare patients unnecessary investigations.

IRB APPROVAL Yes — *IRB Approval Letter may be requested*.

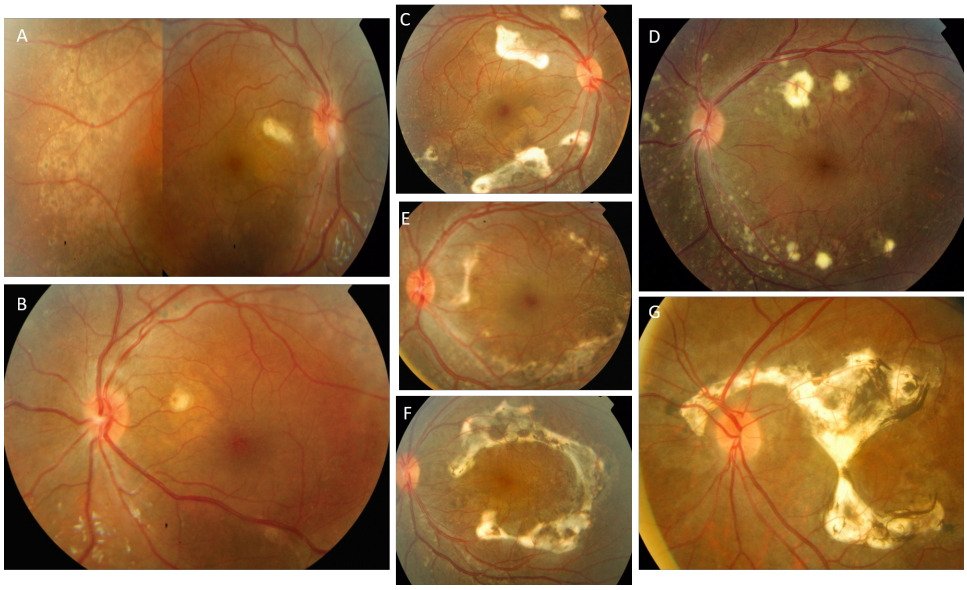

Fundus photographs showing patterns of submacular fibrosis in the enhanced S-cone syndrome (ESCS). A-B: central unifocal nodular fibrosis; C-D: circumferential multifocal nodular fibrosis; E-F: arcuate fibrosis; and G: helicoid fibrosis. Note the near peripheral pigmentary changes characteristic of ESCS in A and B. Note that all the fibrotic lesions are bright and well-demarcated, associated with grayish pigmentation and surrounded by depigmented "halos".